

学会発表に関する一覧

発表者名	演題名	学会名	会場	日時
Inoue N, Ichikawa R, Miyoshi J, Matsuoka K, Hisamatsu T, Okamoto S, <u>Ogata H</u> , Iwao Y, Kanai T, Hibi T	Oral tacrolimus therapy is useful for patients with intractable ulcerative colitis: A result of post-marketing analysis.	15th International Congress of Mucosal Immunology	Paris France	2011年7月5日-9日
Hisamatsu T, Uo M, Miyoshi J, Yoneno K, Inoue N, <u>Ogata H</u> , Kanai T, Hibi T	Intestinal CXCR4+IgG+ immature plasma cells contribute to the pathogenesis of ulcerative colitis through IgG immune complex-Fc γ R signaling.	15th International Congress of Mucosal Immunology	Paris France	2011年7月5日-9日
Miyoshi J, Yajima T, Okamoto S, Matsuoka K, Inoue N, Hisamatsu T, Shimamura K, Nakazawa A, Kanai T, <u>Ogata H</u> , Iwao Y, Mukai M, Hibi T	Ectopic expression of blood type antigens in inflamed mucosa with higher incidence of FUT2 secretor status in colonic Crohn's disease.	15th International Congress of Mucosal Immunology	Paris France	2011年7月5日-9日
Kimura K, Kanai T, Bessho R, Hosoe N, Kobayashi T, Takayama T, Inoue N, Mukai M, <u>Ogata H</u> , and Hibi T	In vivo visualization and evaluation of colorectal inflammation in ulcerative colitis by a newly integrated endocytoscopy.	Digestive Disease Week2011	Chicago	2011年5月7日-10日
細江直樹、柏木和弘、井上詠、岩男泰、緒方晴彦、今枝博之、碓井真吾、日比紀文	内視鏡的小腸ポリープ切除におけるアンカークリップの有用性	第93回日本消化器内視鏡学会関東地方会	東京	2011年12月10日
村田宏子、石橋由佳、木村佳代子、米野和明、碓井真吾、日比紀文、細江直樹、柏木和弘、緒方晴彦、今枝博之	複数回のバルーン内視鏡、カプセル内視鏡により病変を同定し得た Pyogenic granuloma の一例	第93回日本消化器内視鏡学会関東地方会	東京	2011年12月9日
柏木和弘、細江直樹、井上詠、岩男泰、緒方晴彦、梅田瑠美子、高林馨、日比紀文、今枝博之	大腸内視鏡挿入困難例に対するバルーン内視鏡の臨床的有用性	第93回日本消化器内視鏡学会関東地方会	東京	2011年12月9日
水上健、今井仁、今村論、清水智樹、長久保秀一、諸星雄一、藤田由里子、小松弘一、今枝博之、緒方晴彦、日比紀文	挿入困難例における先端柔軟構造大腸鏡の有用性—コロンモデルにおけるヘアピン通過と深部挿入性の提示—	第93回日本消化器内視鏡学会関東地方会	東京	2011年12月9日
三好潤、松岡克善、井上詠、久松理一、米野和明、金井隆典、緒方晴彦、岩男泰、日比紀文	難治性潰瘍性大腸炎に対するタクロリム経口投与の治療効果	第66回日本大腸肛門病学会学術集会	東京	2011年11月26日
松岡克善、岩男泰、井上詠、久松理一、金井隆典、緒方晴彦、日比紀文	潰瘍性大腸炎に合併する大腸癌/dysplasiaの臨床的検討	第66回日本大腸肛門病学会学術集会	東京	2011年11月26日
水上健、緒方晴彦、日比紀文	先端柔軟構造大腸鏡の『浸水法』による運用	第82回日本消化器内視鏡学会総会	福岡	2011年10月23日
細江直樹、緒方晴彦、日比紀文	大腸用カプセル内視鏡による潰瘍性大腸炎患者の病勢評価	第82回日本消化器内視鏡学会総会	福岡	2011年10月22日
米野和明、久松理一、岡本晋、松岡克善、市川理子、筋野智久、三好潤、三上洋平、高山哲朗、矢島知治、井上詠、岩男泰、金井隆典、緒方晴彦、日比紀文	クローン病インフリキシマブ投与症例における長期治療成績の検討	第53回日本消化器病学会大会	福岡	2011年10月20日
丸山悠里子、松岡克善、岩男泰、矢島知治、井上詠、久松理一、筋野智久、高林馨、米野和明、三上洋平、三好潤、水野慎大、木村佳代子、金井隆典、緒方晴彦、日比紀文	難治性潰瘍性大腸炎における cytomegalovirus再活性化例の検討	第53回日本消化器病学会大会	福岡	2011年10月20日
松岡克善、長沼誠、市川仁志、井上詠、小林拓、岡本晋、久松理一、金井隆典、緒方晴彦、岩男泰、日比紀文	潰瘍性大腸炎治療における Endoscopic activity (EAI) の有用性	第29回日本大腸検査学会総会	東京	2011年9月18日

学会発表に関する一覧

発表者名	演題名	学会名	会場	日時
細江直樹、松岡克善、今枝博之、石橋由佳、木村佳代子、岡田佐和子、米野和明、碓井真吾、井田陽介、久松理一、井上詠、岩男泰、日比紀文、緒方晴彦	大腸用カプセル内視鏡による潰瘍性大腸炎患者のスクリーニング	第29回日本大腸検査学会総会	東京	2011年9月17日
細江直樹、緒方晴彦、日比紀文	慢性維持透析患者における小腸病変のサーベイランス	第81回日本消化器内視鏡学会総会	名古屋	2011年8月17日
久松理一、鶴尾道秀、米野和明、井上詠、緒方晴彦、金井隆典、日比紀文	粘膜内CXCR4+IgG産生型形質細胞はIgG免疫複合体を介して潰瘍性大腸炎病態に関与する	第48回日本消化器免疫学会総会	金沢	2011年7月21日
金井隆典、筋野智久、松岡克善、米野和明、三上洋平、三好潤、高林馨、丸山ゆり子、水野慎太、木村佳代子、佐藤俊朗、久松理一、矢島知治、井上詠、緒方晴彦、岩男泰、日比紀文	高齢者下部消化管疾患の診療ガイドライン作成に向けて 高齢者炎症性腸疾患のガイドライン作成に向けて	第14回日本高齢消化器病学会学術大会	東京	2011年7月2日
八島史明、丸山悠里子、船越信介、松岡克善、山岸由幸、中村雄二、久松理一、鈴木秀和、金井隆典、岩男泰、日比紀文、細江直樹、緒方晴彦、亀山香織、林雄一郎、三上修治、向井万起男	原因不明の炎症反応高値、腹痛、便通異常をみとめ、診断に難渋した消化管アミロイドーシスの一例	第315回日本消化器病学会 関東支部例会	東京	2011年7月2日
瀧田麻衣子、関恵理、鳩貝健、岸野竜平、岩崎栄典、泉谷幹子、前田憲男、中澤敦、塚田信廣、福原誠一郎、細江直樹、緒方晴彦、日比紀文	カプセル内視鏡の再検により出血所見を捉えたMeckel憩室の一例	第315回日本消化器病学会 関東支部例会	東京	2011年7月2日
和田安代、久松理一、長沼誠、丸山悠里子、松岡克善、井上詠、岡本晋、矢島知治、米野和明、高林馨、筋野智久、三好潤、三上洋平、水野慎太、緒方晴彦、岩男泰、金井隆典、日比紀文	炎症性腸疾患における骨塩量減少の実態調査とリスク因子の解析	第97回日本消化器病学会総会	東京	2011年5月15日
高林馨、金井隆典、筋野智久、小野祐一、水野慎太、木村佳代子、三上洋平、林篤史、土井知光、松岡克善、久松理一、緒方晴彦、日比紀文	Th17細胞はTh17/Th1細胞を介し腸炎惹起性Th1細胞へと変換する	第97回日本消化器病学会総会	東京	2011年5月14日
筋野智久、金井隆典、三上洋平、小野祐一、松岡克善、久松理一、緒方晴彦、日比紀文	炎症性腸管におけるRORγt陽性細胞の関与	第97回日本消化器病学会総会	東京	2011年5月14日
米野和明、岡本晋、久松理一、松岡克善、市川理子、筋野智久、三好潤、三上洋平、高山哲朗、矢島知治、井上詠、岩男泰、金井隆典、緒方晴彦、日比紀文	膿腫合併がクローン病インフリキシマブ治療に与える影響	第97回日本消化器病学会総会	東京	2011年5月13日
三好潤、矢島知治、岡本晋、松岡克善、井上詠、中澤敦、久松理一、島村克好、金井隆典、緒方晴彦、岩男泰、日比紀文	糖鎖抗原に着目した炎症性腸疾患の病態への新規アプローチ腸管上皮における血液型抗原の発現についての検討	第97回日本消化器病学会総会	東京	2011年5月13日
細江直樹、緒方晴彦、日比紀文	カプセル内視鏡による成人発症Henoch-Schoenlein紫斑病の小腸病変の検討	第97回日本消化器病学会総会	東京	2011年5月13日

V. 知的財産権・社会活動報告

知的財産権

種 類	受付（識別）番号	出願日
大腸上皮幹細胞の単離・培養技術と、これを用いた大腸上皮移植技術 (東京医科歯科大学 渡辺 守、中村哲也)	特願2011-236469	2011年10月27日

社会活動に関する一覧表

活動者名（所属施設）	会の名称および講演演題等	会場および新聞名等	活動年月日
渡辺 守 (東京医科歯科大学)	IBDの進歩と近未来像一治る時代へー／第8回 市民公開講座「炎症性腸疾患の治療をめぐる」	奈良 (はぐくみセンター)	2011年12月18日
渡辺 守 (東京医科歯科大学)	潰瘍性大腸炎の克服に向けた「厚生労働省難病研究班」の取り組み／進歩する潰瘍性大腸炎治療	大阪 (堂島リバーフォーラムホール)	2011年11月27日
渡辺 守 (東京医科歯科大学)	潰瘍性大腸炎を知っていますか／健康プラザかつしかオープニングイベント	東京 (健康プラザかつしか)	2011年9月17日
平田一郎 (藤田保健衛生大学)	10～30歳代を中心に急増する潰瘍性大腸炎	朝日新聞朝刊	2011年12月18日
平田一郎 (藤田保健衛生大学)	日本消化器内視鏡学会・北陸地方会・教育講演「薬剤性腸炎, collagenous colitis」	金沢大学	2010年11月21日

VI. 研究事業報告

<最終版>

厚生労働科学研究難治性疾患克服研究事業
「難治性腸管吸収障害Microscopic Colitisに関する調査研究」
平成 23 年度第 1 回総会

期日 平成 23 年 7 月 15 日（金）14 時 30 分～

場所 味の素株本社ビル（東京都中央区京橋1-15-1）

研究代表者 渡辺 守
（東京医科歯科大学消化器病態学）

事務局 東京医科歯科大学消化器病態学

担当 岡本隆一

TEL : 03-5803-5974 FAX : 03-5803-0268

E-mail : rokamoto.gast@tmd.ac.jp

第1回総会について

1) 演題発表について

- (1) スライドは、Power Point で作成し、USB フラッシュメモリディスクまたは CD-ROM に保存したものをお持ち下さい。(Windows, Macintosh どちらも対応可能ですが、御自分の PC 以外の機器でも試写してからお持ち下さい。)
- (2) B1 会場スライド受付までご提出下さい。その際、試写（出力確認）も必ず行ってください。使用したメディアは、画面確認後その場でご返却いたします。
- (3) 発表・報告は3分でお願い致します。

2) 発表データについて

厚生労働省への報告の必要上、発表スライドファイルを当日複製させていただきますことをご了承下さい。不都合のある先生におかれましては、事前に事務局まで御連絡をお願いします。

3) 会場セキュリティについて

- (1) 一階玄関ホール総会受付にて芳名録へご署名後、セキュリティカードをお受け取りいただき、改札を通過して地下一階会場へお進みください。
- (2) 館内はセキュリティ制ですのでセキュリティカードを必ず常時携帯してください。退出される際にはカードをご返却ください。カードの紛失があると全館内のセキュリティに支障を来しますので、くれぐれも紛失ならびにお持ち帰りにならないようご注意ください。

4) 駐車場について

駐車スペースはご用意しておりませんので、公共の交通機関をご利用ください。

5) 会場案内図 味の素(株)本社ビル 東京都中央区京橋 1-15-1 / Tel. 03-5250-8111



- ② 東京メトロ銀座線「京橋駅」6番出口（徒歩5分）
- ③ 都営浅草線「宝町駅」A-2出口（徒歩3分）
- ④ 東京メトロ日比谷線「八丁堀駅」北口（徒歩10分）

厚生労働科学研究難治性疾患克服事業
「難治性腸管吸収障害 Microscopic Colitis に関する調査研究」
平成 23 年度第 1 回総会プログラム

(敬称略、発表予定者は○印)

平成23年7月15日 (金)

開会 (14 : 30)

I. 研究代表者挨拶 (14 : 30～14 : 40)

渡辺 守 (東京医科歯科大学大学院・消化器病態学)

II. 疾患概念と定義 (14 : 40～14 : 55)

○平田一郎 (藤田保健衛生大学・消化管内科学)

II. 実態調査 (14 : 55～15 : 10)

○岡本隆一 (東京医科歯科大学大学院・消化器病態学)

III. 診断基準の策定に向けて (15 : 10～15 : 40)

臨床診断

○松井敏幸 (福岡大学筑紫病院・消化器内科)

清水誠治 (JR 大阪鉄道病院・消化器内科)

病理診断

○原岡誠司 (福岡大学筑紫病院・病理部)

○田中正則 (弘前市立病院・臨床検査科)

IV. 治療指針の策定に向けて (15 : 40～16 : 00)

○松本主之 (九州大学大学院医学研究院・病態機能内科学)

緒方晴彦 (慶應義塾大学医学部・内視鏡センター)

V. 病態の解明に向けて (16 : 00～16 : 20)

○三浦総一郎 (防衛医科大学学校・内科学)

○土屋輝一郎 (東京医科歯科大学大学院・消化器病態学)

○佐藤俊郎¹、緒方晴彦²、日比紀文¹

(慶應義塾大学医学部・消化器内科¹、同 内視鏡センター²)

閉会の挨拶 (16 : 30 終了予定)

VII. 研究成果の別刷り

Functional engraftment of colon epithelium expanded *in vitro* from a single adult Lgr5⁺ stem cell

Shiro Yui^{1,6}, Tetsuya Nakamura^{2,6}, Toshiro Sato^{3,5}, Yasuhiro Nemoto¹, Tomohiro Mizutani¹, Xiu Zheng¹, Shizuko Ichinose⁴, Takashi Nagaishi¹, Ryuichi Okamoto², Kiichiro Tsuchiya¹, Hans Clevers³ & Mamoru Watanabe¹

Adult stem-cell therapy holds promise for the treatment of gastrointestinal diseases. Here we describe methods for long-term expansion of colonic stem cells positive for leucine-rich repeat containing G protein-coupled receptor 5 (Lgr5⁺ cells) in culture. To test the transplantability of these cells, we reintroduced cultured GFP⁺ colon organoids into superficially damaged mouse colon. The transplanted donor cells readily integrated into the mouse colon, covering the area that lacked epithelium as a result of the introduced damage in recipient mice. At 4 weeks after transplantation, the donor-derived cells constituted a single-layered epithelium, which formed self-renewing crypts that were functionally and histologically normal. Moreover, we observed long-term (>6 months) engraftment with transplantation of organoids derived from a single Lgr5⁺ colon stem cell after extensive *in vitro* expansion. These data show the feasibility of colon stem-cell therapy based on the *in vitro* expansion of a single adult colonic stem cell.

Epithelial stem cells maintain tissue homeostasis throughout the gastrointestinal tract^{1–3}. The Wnt, bone morphogenetic protein (BMP) and Notch cascades function together to regulate stem-cell maintenance^{4,5}. *Lgr5* marks stem cells in small intestinal and colonic crypts⁶ and in gastric units⁷. *Bmi1* may mark distinct stem cells in the proximal small intestine⁸. It has been shown that freshly isolated intestinal epithelium can be transplanted in rodents after resident epithelium has been surgically removed^{9,10}. We previously developed a three-dimensional culture technique that allows expansion of single Lgr5⁺ stem cells from small intestine¹¹, stomach⁷ and colon¹². The resulting organoids then expand and self organize into an epithelial architecture that is reminiscent of that seen in *in vivo* histology. Moreover, the growing organoids maintain their tissue identity even after prolonged culture. Here we sought to evaluate whether the cultured Lgr5⁺ cells faithfully represent the tissue-resident Lgr5⁺ stem cells and, thus, are able to regenerate epithelial tissue *in vivo*. Considering that the colon is very vulnerable to disease in humans, we focused on colonic stem cells in our analyses.

RESULTS

Long-term, serum-free culture system for colonic organoids

We subjected the colons of adult mice to a combination of enzymes¹³, reducing agents¹⁴ and mechanical disruption. The resulting crypt fragments were mostly devoid of α smooth muscle actin gene (*Acta2*)-expression-positive non-epithelial components and consisted of a mix of cadherin 1, type 1, E-cadherin (*Cdh1*)⁺ cells expressing terminal differentiation marker genes (*Muc2*, *CA2* and *ChgA*) and Lgr5⁺ stem cells (Supplementary Fig. 1a,b).

The addition of R-spondin 1 (Rspo1), Noggin and epidermal growth factor (EGF), which are all essential to small intestine culture¹¹, did not maintain the growth of colonic crypts. We therefore developed the following ‘TMDU (Tokyo Medical and Dental University) protocol’: we embedded crypts in type I collagen in serum-free medium with Wnt3a, hepatocyte growth factor (HGF)^{15,16} and BSA, in addition to Rspo1, Noggin and EGF (Supplementary Fig. 1c). Sequential imaging of the cultures revealed rapid growth of cystic structures (Fig. 1a). Wnt3a, Rspo1 and BSA were essential to this growth (Supplementary Fig. 1d). As predicted by previous results^{17,18}, Rspo1 could be substituted with Wnt3a (data not shown). Although Noggin, EGF and HGF were not essential for growth of the colonic crypts, each enhanced their growth (Supplementary Fig. 1e). The colonic organoids rarely had buds (Fig. 1a, Supplementary Fig. 2a and Supplementary Video 1). Of note, small intestinal organoids also generate cystic structures when Wnt3a is added to them¹⁹.

The colonic organoids were single layered (Supplementary Fig. 2b), and all the cells within were positive for *Cdh1* expression (Fig. 1b). The basal membranes of the organoids faced outward (Fig. 1b). Ki67⁺ cells were present in the colonic organoids (Fig. 1b), as were alcian blue-positive goblet cells, chromogranin A (ChgA)⁺ enteroendocrine cells, carbonic anhydrase II (CA2)⁺ colonocytes and cytochrome c oxidase subunit I (COX1)⁺ tuft cells²⁰ (Fig. 1b). Transmission electron microscopy revealed epithelial characteristics such as microvilli (Fig. 1c) and junctional complexes (Fig. 1d) in the organoids. However, stromal cells were absent (Supplementary Fig. 2c). Mitotic cells with condensed chromosomes were present in the organoids (Fig. 1e), and goblet cells (Fig. 1f) and enteroendocrine cells (Fig. 1g) could also be clearly detected.

¹Department of Gastroenterology and Hepatology, Graduate School, Tokyo Medical and Dental University, Bunkyo-ku, Tokyo, Japan. ²Department of Advanced Therapeutics for Gastrointestinal Diseases, Tokyo Medical and Dental University, Bunkyo-ku, Tokyo, Japan. ³Hubrecht Institute and University Medical Centre, Utrecht, The Netherlands. ⁴Research Center for Medical and Dental Sciences, Tokyo Medical and Dental University, Bunkyo-ku, Tokyo, Japan. ⁵Present address: Department of Gastroenterology, Keio University School of Medicine, Shinjuku-ku, Tokyo, Japan. ⁶These authors contributed equally to this work. Correspondence should be addressed to H.C. (h.clevers@hubrecht.eu) or M.W. (mamoru.gast@tmd.ac.jp).

Received 30 July 2011; accepted 29 November 2011; published online 11 March 2012; doi:10.1038/nm.2695

TECHNICAL REPORTS

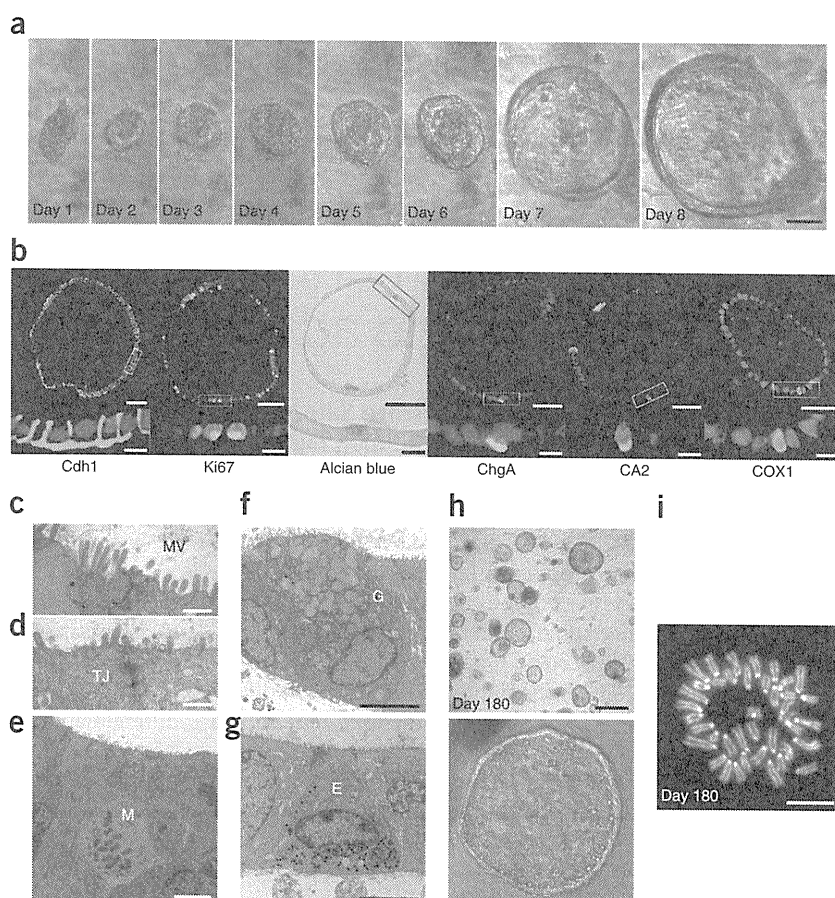
Figure 1 Long-term, serum-free culture of colonic epithelial cells. (a) A representative colonic crypt growing as a cystic structure. Scale bar, 50 μ m. Time-lapse images of another colonic crypt are shown in **Supplementary Figure 2a** and **Supplementary Video 1**.

(b) Histology of the colonic organoids at day 8 of culture. Cdh1⁺ cells, actively proliferating Ki67⁺ cells (green) and terminally differentiated cells stained with alcian blue (blue, goblet cells) or immunostained with ChgA (green, enteroendocrine cells), CA2 (green, colonocytes) or COX1 (green, tuft cells) are shown.

Higher magnification views of the boxed areas are shown at the bottom. DAPI staining was performed, except for the experiments in which we performed alcian blue staining. Scale bars, top, 50 μ m; bottom, 10 μ m. (c–g) Transmission electron microscopy analysis for organoids at day 8. (c,d) Microvilli (MV) and intracellular tight junctions (TJ) are shown. (e) Mitotic (M) cells showing chromatin condensation. (f,g) Goblet cells (G) with mucus granules (f) and enteroendocrine cells (E) with electron dense granules (g) are shown. Scale bars: c,d, 0.5 μ m; e–g, 5 μ m.

Low-power views of f and g are also shown in **Supplementary Figure 2c**. (h) The culture at day 180 (top) and its representative organoid (bottom). Scale bars, top, 500 μ m; bottom, 50 μ m. Images of the growth of a single cell after passage are shown in **Supplementary Figure 3** and **Supplementary Video 2**.

(i) Metaphase spread of a cell at day 180 shows a normal karyotype ($2n = 40$). Scale bar, 10 μ m.



The organoids could be passaged weekly at a 1:2 ratio (**Supplementary Fig. 3** and **Supplementary Video 2**). Addition of the Rho kinase inhibitor Y-27632 (ref. 21) improved the replating efficiency of the organoids¹¹. We successfully propagated organoids

for more than 6 months without clear alterations of morphology (**Fig. 1h**) or karyotype (**Fig. 1i**).

Lgr5⁺ cells are enriched in colonic organoids

We tracked the expression of *Lgr5* over 60 d and found a substantial elevation during the first 8 d of observation (**Fig. 2a**). We found no change in the expression of *ChgA* and *CA2*, whereas *Muc2* expression was repressed in the first 8 d (**Fig. 2a**). Addition of a combination of Wnt3a, Rspo1 and BSA induced *Lgr5* expression (**Fig. 2b**). *Lgr5* expression was further upregulated by the addition of Noggin, which is an antagonist of BMP²² (**Fig. 2b**). The Notch pathway suppresses the

Figure 2 Lgr5⁺ stem cells are enriched in cultured organoids. (a) RT-PCR analysis of the colonic crypts immediately after isolation (crypt) or organoids cultured for 8 or 60 d. *Lgr5* was upregulated and stayed constant thereafter. Differentiation marker genes (*Muc2*, *ChgA* and *CA2*) were expressed over 60 d. The primers used are listed in **Supplementary Table 1**. (b) RT-PCR shows that *Lgr5* upregulation is mediated by a combination of minimum factors (Wnt3a, Rspo1 and BSA) and Noggin but not by EGF and HGF. (c) Notch signal-mediated cell fate determination *in vitro*. Cultured organoids were treated with GSI, LY-411575 or vehicle alone from day 4 to day 8. Organoids stained with alcian blue are shown (left). Scale bar, 50 μ m. RT-PCR shows that the expression of *Muc2* is upregulated, whereas the expression of *Lgr5* is reciprocally downregulated in organoids treated with LY-411575 (GSI, right). Similar results were obtained in three independent experiments, and representative data are shown. (d) A time-lapse imaging of a growing colonic crypt obtained from an *Lgr5-EGFP-ires-CreERT2* mouse over 192 h. The top panel shows EGFP and the bottom panel shows merged images of EGFP and differential interference contrast (DIC). Scale bar, 50 μ m. The corresponding video (**Supplementary Video 3**) and similar results from another example are available as **Supplementary Figure 4a** and **Supplementary Video 4**.

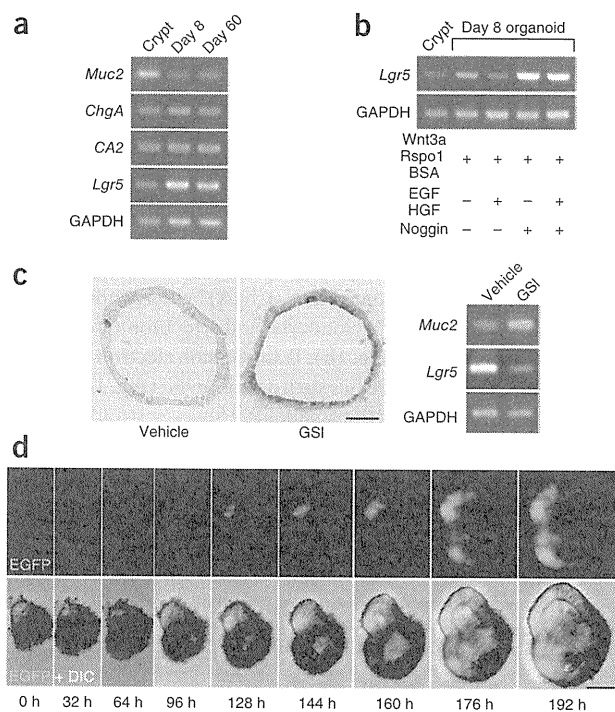


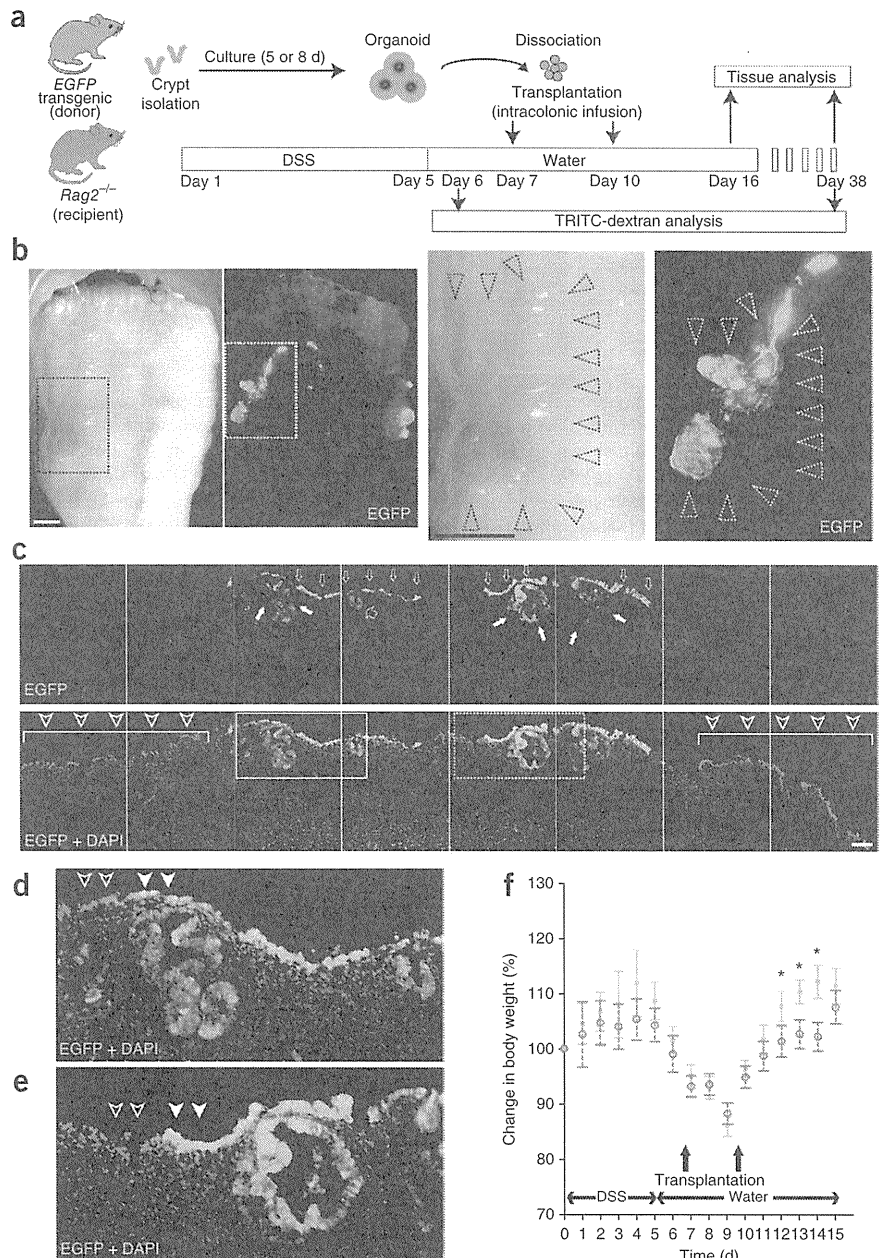
Figure 3 Transplantation of cultured cells improves acute colitis. **(a)** Experimental protocols. **(b)** Recipient colon at 6 d after transplantation. Low-power views (stereoscopic and fluorescent images) are shown on the left. High-power views of the areas in the dotted squares are shown in the right. The black dotted arrowheads show a depressed area surrounded by edematous mucosa. EGFP⁺ areas overlapping the damaged region (white dotted arrowheads) are also shown. Note that the outline of the tissue is not precisely the same in the stereoscopic and fluorescent images, as they were acquired on different microscopes. Scale bars, 1 mm. **(c)** Histology of the EGFP⁺ area shown in **b**. EGFP (top) and the merged image with DAPI staining (bottom). EGFP⁺ cells cover the damaged mucosa that intervene separate areas preserving crypt structures (bottom, arrowheads). EGFP⁺ cells constitute flat linings (top, narrow open arrow) or an invagination (top, wide open arrows), the latter of which is reminiscent of crypts. EGFP⁺ cystic structures were also observed in the EGFP⁺ cells (top, filled white arrows). The regions in the solid- and dotted-line boxes are shown at higher magnification in **d** and **e**, respectively. Scale bar, 100 μ m. **(d)** High-power view of the solid box in **c**. **(e)** High-power view of the dotted box in **c**. **(f)** *Rag2*^{-/-} mice were given DSS for 5 d, and then transplantation ($n = 6$) or sham-transplantation ($n = 6$) was performed. On day 16, the presence of engraftment was retrospectively assessed after the mice were killed. The body weights of the mice with EGFP⁺ engraftment (green squares, $n = 4$) and sham-transplanted controls (red open circles, $n = 6$) are presented as a percentage of their initial weight. Error bars, s.e.m. * $P < 0.05$ (Student's *t* test).

differentiation of progenitors^{23,24} and stem cells²⁵ toward secretory lineages. We treated the colonic organoids with LY-411575, a γ -secretase inhibitor (GSI) that is capable of inhibiting Notch signaling^{26,27}. Notch inhibition induced a goblet-cell phenotype with an increased level of *Muc2* mRNA and a reciprocal decrease in the expression of *Lgr5* (Fig. 2c).

We next performed live imaging of colonic organoids obtained from *Lgr5-EGFP-internal ribosome entry site (ires)-CreERT2* mice⁶ in which an enhanced GFP (EGFP) and tamoxifen-inducible Cre recombinase cassette is integrated into the *Lgr5* locus. The *Lgr5*-promoter-driven EGFP expression initially stayed at a marginal level but then increased beginning at day 5 (Fig. 2d, Supplementary Fig. 4a and Supplementary Videos 3 and 4). We confirmed the expansion of *Lgr5*⁺ cells at a single-cell resolution (Supplementary Fig. 4b). Over multiple passages, the *Lgr5-EGFP* locus tended to become silenced, whereas the wild-type *Lgr5* allele remained active (Fig. 2a,b). Taken together, colonic *Lgr5*⁺ stem cells were able to self renew and expand *in vitro*.

Cultured colonic organoids rescue damaged epithelium

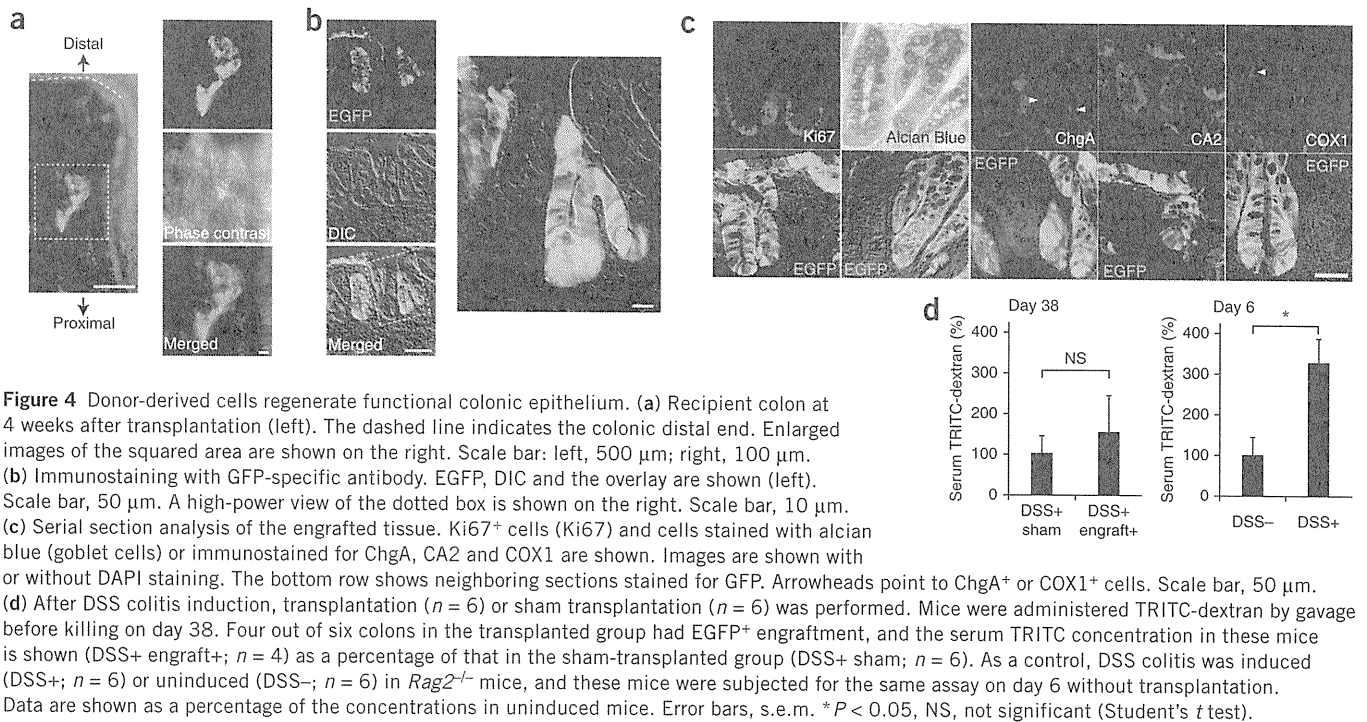
We next tested the transplantability of the cultured organoids (Fig. 3a). We induced colonic mucosal damage by providing immunocompromised *Rag2*^{-/-} mice with colitis-inducing dextran sulfate sodium (DSS)²⁸ for 5 d. Most of the mice developed acute colitis characterized



by weight loss, bloody stool, diarrhea and epithelial injury in the distal colon. At 7 and 10 d after initiating DSS administration, we dissociated the organoids cultured from EGFP transgenic mice²⁹ into small fragments, suspended them in a Matrigel-containing PBS and instilled them by enema in recipient mice.

At 16 d after the start of DSS administration, the recipient colons showed varying degrees of recovery. Multiple EGFP⁺ areas appeared as well-demarcated patches in the treated colons (Fig. 3b). We did not observe any EGFP⁺ areas in colons not treated with DSS (data not shown). Histologically, the EGFP⁺ cells covered the submucosa and were located between the less damaged recipient tissues (Fig. 3c). The EGFP⁺ cells formed flat or slightly invaginated linings (Fig. 3c). We also observed large cystic EGFP⁺ structures below the surface of the treated colons (Fig. 3c). Some of the EGFP⁺ areas connected to the recipients' epithelium (Fig. 3d), whereas others repopulated areas that were devoid of recipient epithelium (Fig. 3e). Notably, the body weights of the mice with engraftment were

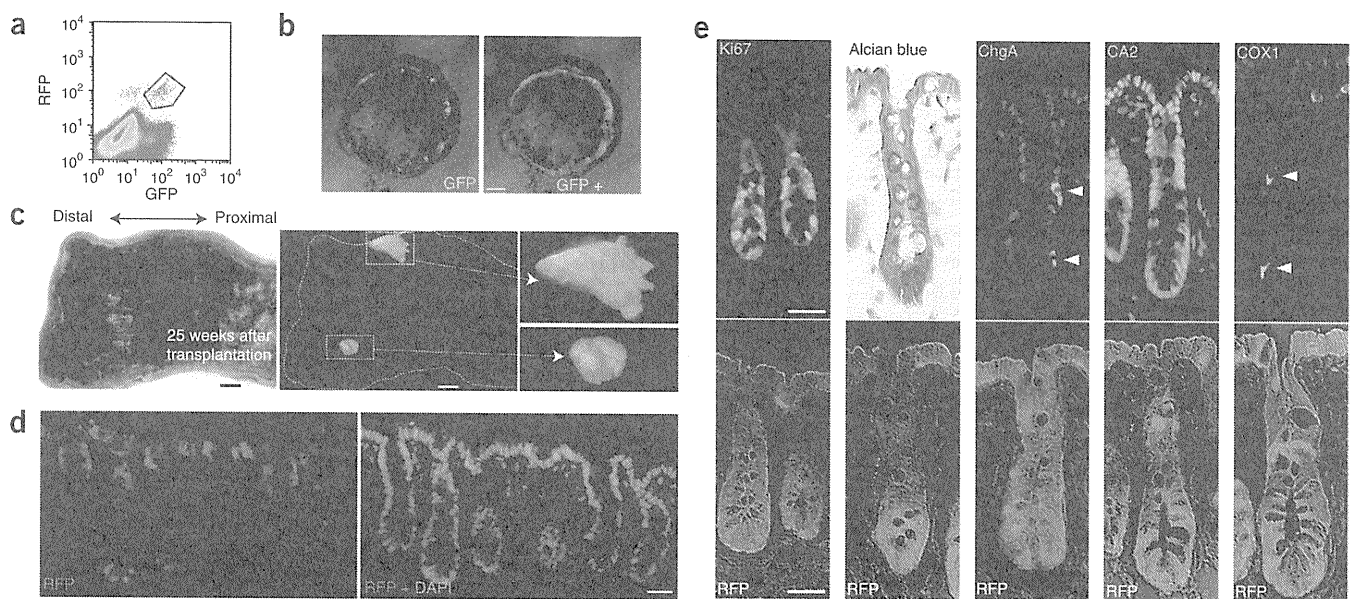
TECHNICAL REPORTS



higher than those of sham-transplanted mice (Fig. 3f; with statistically significant results at days 12, 13 and 14, $P < 0.05$).

At 4 weeks after transplantation, tube-like EGFP⁺ crypts appeared in the distal colon (Fig. 4a) that were morphologically indistinguishable

from the surrounding EGFP⁻ epithelium (Fig. 4b). Notably, the engrafted crypts were entirely EGFP⁺, indicating the presence of EGFP⁺ stem cells (Fig. 4b). Cells in the lower part of the EGFP⁺ crypts were normally Ki67⁺, and the EGFP⁺ crypts contained all



from the surrounding EGFP⁻ epithelium (Fig. 4b). Notably, the engrafted crypts were entirely EGFP⁺, indicating the presence of EGFP⁺ stem cells (Fig. 4b). Cells in the lower part of the EGFP⁺ crypts were normally Ki67⁺, and the EGFP⁺ crypts contained all

terminally differentiated cell types (Fig. 4c). We probed the epithelial permeability of the engrafts using tetramethylrhodamine isothiocyanate (TRITC)-conjugated dextran (TRITC-dextran). Blood TRITC concentrations in transplanted mice were comparable to those in control mice, indicating a maintenance of epithelial barrier function in these engrafts (Fig. 4d). Notably, transplantation was less successful with freshly isolated donor cells ($P < 0.05$, Mann-Whitney U test; Supplementary Fig. 5), suggesting that the expansion of stem cells during the culture is associated with a higher success rate of transplantation. In addition, Matrigel-containing organoid suspensions transplanted better than organoids suspended in PBS (Supplementary Fig. 5; $P < 0.05$, Mann-Whitney U test), proposing a role for the simultaneous supply of extracellular matrix in successful transplantation.

Engraftment of organoids derived from a single Lgr5⁺ cell

We next sought to initiate the protocol described above from a single stem cell (Supplementary Fig. 6a). We crossed *Lgr5-EGFP-ires-CreERT2* mice with *R26R-Confetti* reporter mice³⁰. In the resulting offspring, tamoxifen-induced Cre activation resulted in Cre-mediated recombination at the *Rosa26* locus in individual Lgr5⁺ stem cells, leading to stochastically selected expression of one out of four fluorescent proteins: red fluorescent protein (RFP), cyan fluorescent protein (CFP), GFP or yellow fluorescent protein (YFP). At 3 d after Cre activation, we sorted cells double positive for Lgr5-EGFP and Confetti-RFP, which consisted of ~0.02% of the total cells (Fig. 5a), equivalent to ~100 cells per mouse.

We cultured the sorted cells after a limiting dilution (100 cells per 96 well) using the Hubrecht protocol (Online Methods; protocol described previously¹² with addition of Y-27632 in the first 2 d). Four stem cells double positive for Lgr5-EGFP and Confetti-RFP grew out, which was comparable to the culture efficiency of small intestinal stem cells¹¹ (Fig. 5b). Organoids were expanded to more than 100 wells in >10 weeks, frozen and shipped. After thawing, we recovered the cells under the TMDU protocol. We transplanted ~500 organoids per recipient mouse, as described above. Analyses at 4, 17, 21 and 25 weeks after transplantation revealed the presence of grafts in these mice (Fig. 5c and Supplementary Figs. 6b,c and 7a). At 25 weeks after transplantation, RFP⁺ cells still generated a single-layered epithelium. We noted no sign of adenomatous or dysplastic change in any of the transplanted areas (Fig. 5d). Again, all differentiated cell types, as well as Ki67⁺ proliferating cells, were present at normal ratios (Fig. 5e and Supplementary Fig. 7b).

DISCUSSION

Here we describe methodologies to isolate, culture and transplant Lgr5⁺ colon stem cells. Our observations confirm that *Lgr5* marks genuine stem cells that retain their self-renewal and multilineage-differentiation properties even after prolonged culture. A major difference between small-intestinal and colon-culture conditions is in the latter's requirement for Wnt. Although Wnt factors can initiate Wnt signals on their own, R-spondins (such as Rspo1) can only augment preexisting Wnt signals³¹. Because Paneth cells produce Wnt3, they serve as the center of organization of the stem cell niche¹⁹. At the colon crypt bottoms, secretory cells are located between the Lgr5⁺ stem cells that—like Paneth cells—express CD24 (ref. 19). However, these CD24⁺ secretory cells do not produce a sufficient amount of Wnt proteins *in vitro* (data not shown). Therefore, colon organoids cannot grow from Rspo1 alone but, rather, also require exogenous Wnt.

This study provides proof of principle that cultured Lgr5⁺ cells can be used for stem-cell therapy to repair damaged epithelium.

Transplanted cells adhere to and cover superficially damaged tissue. Further, engrafted recipient mice had higher body weights than ungrafted controls, implying a beneficial role for the donor cells in DSS-induced acute colitis. Although further optimization is clearly needed, the current study implies that *in vitro* expansion and transplantation of gastrointestinal stem cells may be a promising option for patients with severe gastrointestinal epithelial injuries.

Lgr5⁺ stem cells divide once every day *in vivo*⁶, thus defying the Hayflick limit³². They appear similarly unrestricted in their proliferative capacity *in vitro*, while they retain their original tissue identity. It is of interest that the Lgr5 protein is now known to reside in the Wnt receptor complex to function as a receptor for Rspo1 (refs. 33,34), which is a crucial component of long-term organoid culture systems that we have developed. As the resulting organoids have now been proven to be transplantable, the Lgr5⁺ stem cell isolation and expansion technology may provide a simple and safe avenue for the development of new regenerative and gene-therapy strategies.

METHODS

Methods and any associated references are available in the online version of the paper at <http://www.nature.com/naturemedicine/>.

Note: Supplementary information is available on the Nature Medicine website.

ACKNOWLEDGMENTS

We thank M. Okabe (Osaka University) for EGFP transgenic mice and Y. Kato, J. Inazawa, I. Sekiya (TMDU), H. Snippert and R. Vries (Hubrecht Institute) for technical assistance. This study was supported by Grant-in-Aid for Scientific Research from the Japanese Ministry of Education, Culture, Sports, Science and Technology, by the Health and Labour Sciences Research Grants for Research on Intractable Diseases from Ministry of Health, Labour and Welfare of Japan, and by a grant from the European Research Council and from the Dutch Cancer Foundation.

AUTHOR CONTRIBUTIONS

T. Nakamura, H.C. and M.W. designed the study. S.Y., T. Nakamura and T.S. performed experiments and analyzed data. T. Nakamura, T.S. and H.C. wrote the paper. Y.N., T. Nagaishi and K.T. assisted in transplantation experiments. T.M., X.Z. and K.T. gave support in gene analysis. R.O. helped with the immunohistochemistry. S.I. advised on the electron microscopy. H.C. and M.W. gave conceptual advice and supervised the project.

COMPETING FINANCIAL INTERESTS

The authors declare competing financial interests: details accompany the full-text HTML version of the paper at <http://www.nature.com/naturemedicine/>.

Published online at <http://www.nature.com/naturemedicine/>.

Reprints and permissions information is available online at <http://www.nature.com/reprints/index.html>.

- Potten, C.S., Booth, C. & Pritchard, D.M. The intestinal epithelial stem cell: the mucosal governor. *Int. J. Exp. Pathol.* **78**, 219–243 (1997).
- Bjerknes, M. & Cheng, H. Intestinal epithelial stem cells and progenitors. *Methods Enzymol.* **419**, 337–383 (2006).
- Barker, N., van de Wetering, M. & Clevers, H. The intestinal stem cell. *Genes Dev.* **22**, 1856–1864 (2008).
- Crosnier, C., Stamatakis, D. & Lewis, J. Organizing cell renewal in the intestine: stem cells, signals and combinatorial control. *Nat. Rev. Genet.* **7**, 349–359 (2006).
- Radtke, F. & Clevers, H. Self-renewal and cancer of the gut: two sides of a coin. *Science* **307**, 1904–1909 (2005).
- Barker, N. *et al.* Identification of stem cells in small intestine and colon by marker gene *Lgr5*. *Nature* **449**, 1003–1007 (2007).
- Barker, N. *et al.* Lgr5⁺ stem cells drive self-renewal in the stomach and build long-lived gastric units *in vitro*. *Cell Stem Cell* **6**, 25–36 (2010).
- Sangiorgi, E. & Capecchi, M.R. *Bmi1* is expressed *in vivo* in intestinal stem cells. *Nat. Genet.* **40**, 915–920 (2008).
- Avansino, J.R., Chen, D.C., Woolman, J.D., Hoagland, V.D. & Stelzner, M. Engraftment of mucosal stem cells into murine jejunum is dependent on optimal dose of cells. *J. Surg. Res.* **132**, 74–79 (2006).
- Tait, I.S., Evans, G.S., Flint, N. & Campbell, F.C. Colonic mucosal replacement by syngeneic small intestinal stem cell transplantation. *Am. J. Surg.* **167**, 67–72 (1994).

TECHNICAL REPORTS

11. Sato, T. *et al.* Single Lgr5 stem cells build crypt-villus structures *in vitro* without a mesenchymal niche. *Nature* **459**, 262–265 (2009).
12. Sato, T. *et al.* Long-term expansion of epithelial organoids from human colon, adenoma, adenocarcinoma, and Barrett's epithelium. *Gastroenterology* **141**, 1762–1772 (2011).
13. Booth, C., Patel, S., Bennion, G.R. & Potten, C.S. The isolation and culture of adult mouse colonic epithelium. *Epithelial Cell Biol.* **4**, 76–86 (1995).
14. Whitehead, R.H., Demmler, K., Rockman, S.P. & Watson, N.K. Clonogenic growth of epithelial cells from normal colonic mucosa from both mice and humans. *Gastroenterology* **117**, 858–865 (1999).
15. Kanayama, M. *et al.* Hepatocyte growth factor promotes colonic epithelial regeneration via Akt signaling. *Am. J. Physiol. Gastrointest. Liver Physiol.* **293**, G230–G239 (2007).
16. Tahara, Y. *et al.* Hepatocyte growth factor facilitates colonic mucosal repair in experimental ulcerative colitis in rats. *J. Pharmacol. Exp. Ther.* **307**, 146–151 (2003).
17. Kim, K.A. *et al.* Mitogenic influence of human R-spondin1 on the intestinal epithelium. *Science* **309**, 1256–1259 (2005).
18. Wei, Q. *et al.* R-spondin1 is a high affinity ligand for LRP6 and induces LRP6 phosphorylation and β -catenin signaling. *J. Biol. Chem.* **282**, 15903–15911 (2007).
19. Sato, T. *et al.* Paneth cells constitute the niche for Lgr5 stem cells in intestinal crypts. *Nature* **469**, 415–418 (2011).
20. Gerbe, F. *et al.* Distinct ATOH1 and Neurog3 requirements define tuft cells as a new secretory cell type in the intestinal epithelium. *J. Cell Biol.* **192**, 767–780 (2011).
21. Watanabe, K. *et al.* A ROCK inhibitor permits survival of dissociated human embryonic stem cells. *Nat. Biotechnol.* **25**, 681–686 (2007).
22. Haramis, A.P. *et al.* *De novo* crypt formation and juvenile polyposis on BMP inhibition in mouse intestine. *Science* **303**, 1684–1686 (2004).
23. Fre, S. *et al.* Notch signals control the fate of immature progenitor cells in the intestine. *Nature* **435**, 964–968 (2005).
24. van Es, J.H. *et al.* Notch/ γ -secretase inhibition turns proliferative cells in intestinal crypts and adenomas into goblet cells. *Nature* **435**, 959–963 (2005).
25. van Es, J.H., de Geest, N., van de Born, M., Clevers, H. & Hassan, B.A. Intestinal stem cells lacking the Math1 tumour suppressor are refractory to Notch inhibitors. *Nat. Commun.* **1**, 18 (2010).
26. Wong, G.T. *et al.* Chronic treatment with the γ -secretase inhibitor LY-411,575 inhibits β -amyloid peptide production and alters lymphopoiesis and intestinal cell differentiation. *J. Biol. Chem.* **279**, 12876–12882 (2004).
27. Okamoto, R. *et al.* Requirement of Notch activation during regeneration of the intestinal epithelia. *Am. J. Physiol. Gastrointest. Liver Physiol.* **296**, G23–G35 (2009).
28. Wirtz, S., Neufert, C., Weigmann, B. & Neurath, M.F. Chemically induced mouse models of intestinal inflammation. *Nat. Protoc.* **2**, 541–546 (2007).
29. Okabe, M., Ikawa, M., Kominami, K., Nakanishi, T. & Nishimune, Y. 'Green mice' as a source of ubiquitous green cells. *FEBS Lett.* **407**, 313–319 (1997).
30. Snippert, H.J. *et al.* Intestinal crypt homeostasis results from neutral competition between symmetrically dividing Lgr5 stem cells. *Cell* **143**, 134–144 (2010).
31. Binnerts, M.E. *et al.* R-Spondin1 regulates Wnt signaling by inhibiting internalization of LRP6. *Proc. Natl. Acad. Sci. USA* **104**, 14700–14705 (2007).
32. Hayflick, L. & Moorhead, P.S. The serial cultivation of human diploid cell strains. *Exp. Cell Res.* **25**, 585–621 (1961).
33. de Lau, W. *et al.* Lgr5 homologues associate with Wnt receptors and mediate R-spondin signalling. *Nature* **476**, 293–297 (2011).
34. Carmon, K.S., Gong, X., Lin, Q., Thomas, A. & Liu, Q. R-spondins function as ligands of the orphan receptors LGR4 and LGR5 to regulate Wnt/ β -catenin signaling. *Proc. Natl. Acad. Sci. USA* **108**, 11452–11457 (2011).

ONLINE METHODS

Mice. *Rag2*^{-/-} mice were from Taconic Farms and Central Laboratories for Experimental Animals. *EGFP* transgenic mice²⁹, *Lgr5-EGFP-ires-CreERT2* mice⁶ and *R26R-Confetti* mice³⁰ are described elsewhere. Male and female mice were randomly used for all experiments. All animal experiments were performed with the approval of the Institutional Animal Care and Use Committee of TMDU.

TMDU protocol for crypt isolation and three-dimensional culture. The colonic tissue was minced and digested. The crypts were further purified by mechanical disruption and density gradient centrifugation. A total of 2,000 crypts were suspended in 200 μ l of the collagen type I solution (Nitta Gelatin Inc.) and placed in 48-well plates. After polymerization, 500 μ l of Advanced DMEM/F12 containing BSA (Sigma), mouse EGF (mEGF) (PeproTech), mWnt3a, mRspo1, mHGF and mNoggin (all from R&D Systems) was added (TMDU medium). For passage, the gel was digested, and then the organoids were disaggregated with EDTA. The dissociated organoids were mixed in type I collagen solution and used for culture. A Rho kinase inhibitor, Y-27632, was added for the first 2 d after the cells were propagated. Where indicated, to induce goblet cell differentiation, organoids were treated with LY-411575, a GSL. See details in the **Supplementary Methods**.

Chromosome analysis. Chromosome karyotyping was performed according to a standard protocol as detailed in the **Supplementary Methods**.

Stereomicroscopy, phase-contrast imaging and histology. Images were acquired on either a fluorescence microscope equipped with phase-contrast setting (BZ-8000, KEYENCE), a fluorescent stereomicroscope system MVX10 (Olympus) or a fluorescence microscope DeltaVision system (Applied Precision). For histology and immunohistochemistry, tissues and organoids were fixed, sequentially dehydrated in sucrose in PBS, and frozen in OCT compound (Tissue Tek). Cryosections were examined by conventional H&E, alcian blue staining and a spectrum of immunohistochemical reactions, as detailed in the **Supplementary Methods**.

Transmission electron microscopy. Transmission electron microscopy was performed in a standard fashion and is detailed in the **Supplementary Methods**.

Live imaging. Live imaging was performed on the DeltaVision system. A culture dish placed on the microscope stage was covered with a chamber in which a humidified premixed gas consisting of 5% CO₂ and 95% air was infused, and the whole setup was set at 37 °C. DIC and fluorescent images were acquired at 20-min intervals. The data were processed using Softworx (Applied Precision) and, if necessary, image editing was performed using Adobe Photoshop Elements 7.0.

Semi-quantitative RT-PCR. Semi-quantitative RT-PCR was performed in standard fashion. The primer sequences used are listed in **Supplementary**

Table 1. PCR products were separated on agarose gels and visualized using ImageQuant TL system (GE Healthcare).

Sorting and Hubrecht-protocol culture for single *Lgr5*⁺ cells. Tamoxifen was injected into *R26R-Confetti* mice crossed with *Lgr5-EGFP-ires-CreERT2* mice, and the colonic crypts from the resulting mice were isolated 3 d later. Epithelial cells were dissociated with TrypLE express (Invitrogen) and analyzed by MoFlo (DakoCytomation). Viable single cells were gated, and then the cells doubly positive for EGFP and RFP were sorted and embedded in Matrigel (BD Bioscience) on 96-well plates. An Advanced DMEM/F12 culture medium supplemented with penicillin and streptomycin, 4-(2-hydroxyethyl)-1-piperazineethanesulfonic acid (HEPES), glutamax, N2, B27 (all from Invitrogen) and growth factors (EGF, noggin and R-spondin) was diluted 1:1 with Wnt3a-conditioned medium and used as Hubrecht medium. Y-27632 was included for the first 2 d to avoid anoikis. Growth factors were added every other day, and the entire medium was changed every 4 d. See the **Supplementary Methods** for additional details.

Transplantation experiments. For the EGFP⁺ cell transplantations, cells isolated from colon tissues were cultured for 5 or 8 d according to the TMDU protocol and used as donor cells. For single *Lgr5*⁺-cell-derived organoid transplantation, cells were expanded based on the Hubrecht protocol and then cryopreserved. The cells were then shipped, thawed and further cultured. Acute colitis was induced by feeding 6-week-old *Rag2*^{-/-} mice with 3.0% DSS (molecular weight 10,000; Ensuiko Sugar Refining Co.) dissolved in drinking water for 5 d (days 1–5). At 7 and 10 d after the start of DSS administration, donor cells equivalent to those from ~500 organoids were instilled into colonic lumen as a suspension. After infusion, the anal verge was glued for 6 h. After the transplantation on day 10, mice were maintained as usual before they were killed and analyzed. See the **Supplementary Methods** for additional details.

TRITC-dextran permeability assay. Intestinal permeability was assessed by enteral administration of TRITC-dextran (molecular mass 4.4 kDa; Sigma). Transplanted or sham-transplanted mice were gavaged with TRITC-dextran 4 h before killing on day 38. Whole blood was obtained at the time of killing, and then the colonic tissues were examined for whether the EGFP⁺ engrafts were present. TRITC-dextran measurements were performed on an ARVO MX (PerkinElmer), with serial dilutions of TRITC-dextran used as a standard curve.

Statistical analyses. Data are shown as means \pm s.e.m. Data for **Figures 3f, 4d** and **Supplementary Figure 7b** were statistically analyzed by the two-sample Student's *t* test. The data for **Supplementary Figure 5** showed non-normal distributions and were analyzed by Mann-Whitney *U* test. Statistical significance for comparisons was assigned at *P* < 0.05.

Additional methods. Detailed methodology is described in the **Supplementary Methods**.



Contents lists available at SciVerse ScienceDirect

Biochemical and Biophysical Research Communications

journal homepage: www.elsevier.com/locate/ybbrc

Real-time analysis of P-glycoprotein-mediated drug transport across primary intestinal epithelium three-dimensionally cultured *in vitro*

Tomohiro Mizutani^{a,1}, Tetsuya Nakamura^{b,*}, Ryo Morikawa^a, Masayoshi Fukuda^a, Wakana Mochizuki^a, Yuhki Yamauchi^a, Kengo Nozaki^a, Shiro Yui^a, Yasuhiro Nemoto^a, Takashi Nagaishi^a, Ryuichi Okamoto^b, Kiichiro Tsuchiya^a, Mamoru Watanabe^a

^a Department of Gastroenterology and Hepatology, Graduate School, Tokyo Medical and Dental University, 1-5-45 Yushima, Bunkyo-ku, Tokyo 113-8519, Japan

^b Department of Advanced Therapeutics for GI Diseases, Graduate School, Tokyo Medical and Dental University, 1-5-45 Yushima, Bunkyo-ku, Tokyo 113-8519, Japan

ARTICLE INFO

Article history:

Received 30 January 2012

Available online xxxx

Keywords:

P-glycoprotein

Drug transport

Intestinal absorption

Cell membrane permeability

Primary culture

Live imaging

ABSTRACT

P-glycoprotein (P-gp) is an efflux transporter that regulates bioavailability of orally administered drugs at the intestinal epithelium. To develop an *in vitro* experimental model that mimics P-gp-mediated intestinal drug transport *in vivo*, we employed normal intestinal epithelium three-dimensionally cultured. Physiological expression of P-gp mRNA and the expression of its protein at the apical membrane were observed in the small intestinal epithelium grown as cystic organoids. Rhodamine123 (Rh123), a substrate for P-gp, was actively transported in the basoapical direction and accumulated in the luminal space, while the epithelial integrity was kept intact. Furthermore, we were able to monitor the whole process of Rh123 transport and its inhibition by verapamil in real-time, from which kinetic parameters for Rh123 transport could be estimated by a mathematical modeling. The method here described to evaluate the dynamics of P-gp-mediated transport in primary intestinal epithelial cells would be instrumental in investigating the physiological function of P-gp and its inhibitors/inducers *in vitro*.

© 2012 Elsevier Inc. All rights reserved.

1. Introduction

Bioavailability of many clinically relevant drugs is modulated by the activity of efflux transporters expressed in the epithelial lining of the intestine [1,2]. P-glycoprotein (P-gp, also known as ABCB1), a member of the ATP-binding cassette family of transporters, is located in the apical membrane of intestinal epithelial cells [3,4] and serves as an important determinant of the disposition of many orally administered drugs [5–9]. There is, thus, a considerable interest in predicting the P-gp-mediated elimination of drug candidates and assessing the drug–drug interactions involving P-gp substrates and inhibitors/inducers in the intestinal epithelium.

Various model systems have been reported to assess the intestinal epithelial drug transport *in vitro*. Among these, cell based assays using human tumor-derived cell lines, such as Caco-2 cells, are the most commonly used method in many laboratories [10]. When grown on a membrane placed between two chambers, those cells form a well-polarized monolayer joined by tight junctions, providing a selective barrier that can be used to study influx (from

the apical to the basal) and efflux (from the basal to the apical) transport of P-gp substrates [11–14]. Although such cell based systems have been well characterized and used as standard assays, several factors, such as variable expression of P-gp in those immortalized cell lines, are known to cause inter-experimental variability of the data [15,16]. Therefore, it would be of importance to develop an experimental model in which drug transport can be assessed in a reliable manner relevant to the physiological *in vivo* function of intestinal epithelium.

Recently, the long-awaited method for *in vitro* culture of normal intestinal epithelium has been developed [17]. When isolated and placed three-dimensionally, the intestinal crypts keep proliferating, forming enclosed structures with their upper openings closed. These “organoids” are lined by an epithelial monolayer containing both immature cells and terminally differentiated cells, with their apical membranes facing the luminal space inside. In light of this, we were particularly interested in determining whether this newly developed culture technology could be adapted for use in drug transport analysis.

In the present study, by developing a real-time imaging system and its mathematical modeling, we show that the primary culture of small intestinal epithelium would serve as an efficient tool to evaluate the dynamics of P-gp-mediated drug transport.

* Corresponding author. Fax: +81 3 5803 0268.

E-mail address: nakamura.gast@tmd.ac.jp (T. Nakamura).

¹ These authors contributed equally.

2. Materials and methods

2.1. 3D culture of intestinal epithelium

Culture of intestinal epithelium was performed as described previously [17]. Crypts of proximal small intestine were obtained from adult C57BL/6 mice and purified. They were counted and embedded in Matrigel (BD Biosciences) at 10,000 crypts/ml. For conventional culture, 30 μ l of Matrigel was seeded on 24-well plates. For live imaging experiments, 60 μ l of Matrigel was placed on 40-mm coverslips placed in 60-mm culture dishes. After the Matrigel solidified, advanced DMEM/F12 medium (Invitrogen) containing 20 ng/ml EGF (Peprotech), 100 ng/ml Noggin, 500 ng/ml R-spondin1 (R&D systems), 2 mM L-glutamine (GIBCO) and penicillin/streptomycin was overlaid. The medium was changed every 4 days. When necessary, Rh123, FITC-dextran, or verapamil (Sigma–Aldrich) was added to the medium as indicated. Animal experiments were performed with the approval of the Institutional Animal Care and Use Committee of Tokyo Medical and Dental University.

2.2. Semi-quantitative RT-PCR

Organoids were isolated from the Matrigel using BD Cell recovery solution as instructed by the manufacturer. Total RNA was isolated and 300 ng was used for cDNA synthesis in a 21 μ l of reaction. 1 μ l of cDNA was amplified by PCR in a 25 μ l reaction. Sense (S) and antisense (AS) primers, and the cycle numbers for the amplification of each gene were as follows: S: 5'-TGCTGTGATTTTCAGAACAA-3' and AS: 5'-TCCAACATATTCGGCTTAG-3' for Abcb1a (22 cycles); and S: 5'-CTGGCCAAGTTCATCCATGA-3' and AS: 5'-GCCATGAGTCCACCACCCTG-3' for Gapdh (19 cycles). PCR products were separated on agarose gels and visualized using Image Quant TL system (GE Healthcare).

2.3. Immunohistochemistry

Tissues and organoids were fixed, dehydrated in 20% sucrose/PBS, and frozen in OCT compound (Tissue Tek). Cryosections (6 μ m thick) were immunostained with an anti-Mdr antibody (1 μ g/ml, Santa Cruz Biotechnology) and a fluorescent secondary antibody (Alexa Fluor 588, Molecular Probes). The sections were also counterstained with DAPI (Vector Laboratories) to visualize nuclei. Images were acquired on a fluorescence microscope DeltaVision system (Applied Precision).

2.4. Live imaging

The isolated crypts were mixed with Matrigel and placed on 40-mm glass coverslips so that the whole gel would be as thin as possible (<1 mm). On Day 3, the coverslip was incorporated into the FCS-2 closed cell chamber (Biopetechs), the thickness of which was set at 1 mm. The chamber was fixed on the stage of a DeltaVision microscope system covered with a thermally-controlled enclosure set at 37 °C. Spherical organoids with diameters of around 50 μ m were chosen and imaged using a fluorescent microscope IX-71 (Olympus) equipped with a xenon light source, a UplansApo 10x objective (0.4 numerical aperture), a 490/20-nm excitation filter, a 528/38-nm filter, and a Cool Snap ES2 digital camera (Roper Scientific). Differential interference contrast (DIC) and fluorescent images were acquired at 3 min intervals. Exposure times were 0.2 s for DIC and 0.03 s for fluorescent images, respectively, with 1 \times 1 binning and an image size of 512 \times 512 pixels. These conditions were kept throughout all experiments. Immediately after the third time frame of imaging (6 min after the start), 5 ml of pre-warmed medium containing Rh123 (1 μ M), with or without various concentration of verapamil, was rapidly infused

from one port on the side of the chamber, allowing the preexisting medium inside to direct out of the chamber from the other side. This enabled a rapid replenishment of medium with no disturbance of the position or morphology of the organoids. All experiments were performed for 5 h and 30 min.

2.5. Data analysis and mathematical modeling

Images at individual time points of all organoids were quantitatively assessed using the SoftWoRx (Applied Precision). For individual images, circular areas with a diameter of 30 μ m were manually set inside (luminal space) and outside (culture medium) of the organoid, and the fluorescent signal for each compartment was expressed by average pixel values of the circular area. The outer intensities (culture medium) of the images acquired immediately before (0 μ M) and after (1 μ M) the Rh123 addition were applied for calculating the concentration of all other areas of a given experiment.

For mathematical modeling, we made an assumption that Rh123 concentration in the lumen is determined only by active inward transport and passive bidirectional diffusion, both of which take place at the inner apical membrane. When Rh123 concentration (1 μ M) remains stable in the donor side due to the excessively large volume in space, the rate of active transport in the basal to apical direction, V_{in} (nmol/s), can be expressed as below:

$$V_{in} = P_{app,active} \cdot S \cdot C_{out} \quad (1)$$

In this equation (Eq. (1)), $P_{app,active}$ (cm/s) is the apparent permeability coefficient of active basoapical transport, S (cm²) is the area of inner surface of the organoids, and C_{out} (μ mol/litter; nmol/cm³) is the outer concentration of Rh123 given as 1. Passive diffusion of Rh123 can occur in both directions, depending on the concentration gradient across the apical membrane. When V_{out} (nmol/s) is defined as the rate of diffusion in the apical to basal direction, it is derived from an equation,

$$V_{out} = P_{app,passive} \cdot S \cdot (C_{in}(t) - C_{out}) \quad (2)$$

where $P_{app,passive}$ (cm/s) is the apparent permeability coefficient of bidirectional passive diffusion, S (cm²) is the inner surface area, and C_{in} (nmol/cm³) is the luminal Rh123 concentration that can be defined as a function of time t . The total amounts of Rh123, transported across the apical membrane inward and outward by a given time t , can be expressed as integral functions $Q_{in}(t)$ and $Q_{out}(t)$, respectively.

$$Q_{in}(t) = \int_0^t V_{in} dt = V_{in} \cdot t \quad (3)$$

$$Q_{out}(t) = \int_0^t V_{out} dt \quad (4)$$

Eq. (1) and (2) can be substituted into Eq. (3) and (4), respectively, to convert equations as below:

$$Q_{in}(t) = P_{app,active} \cdot S \cdot C_{out} \cdot t \quad (5)$$

$$Q_{out}(t) = P_{app,passive} \cdot S \cdot \int_0^t C_{in}(t) dt - P_{app,passive} \cdot S \cdot C_{out} \cdot t \quad (6)$$

The luminal spatial volume, Vol (cm³), can be assumed to stay unchanged during the imaging and, thus, $C_{in}(t)$ can also be expressed as below:

$$C_{in}(t) = \frac{Q_{in}(t) - Q_{out}(t)}{Vol} \quad (7)$$

From Eq. (5)–(7), $C_{in}(t)$ can now be solved as a function of the variable t .

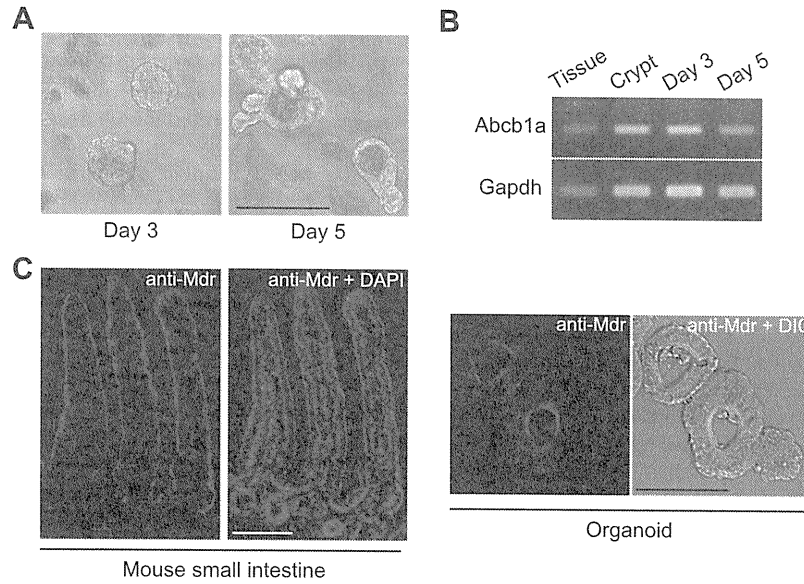


Fig. 1. Physiological expression of P-gp in cultured small intestinal organoids. (A) Phase contrast images of small intestinal organoids on Day 3 (left) and Day 5 (right) of culture. Scale bar, 100 μm . (B) Expression of P-gp (*Abcb1a*) mRNA analyzed by semi-quantitative RT-PCR. Expression levels in the whole small intestine (tissue), isolated crypts (crypt), and the organoids on Day 3 and Day 5 are shown (top). PCR products for *Gapdh* are shown as internal controls (bottom). (C) Localization of P-gp proteins. Immunohistochemistry with an anti-Mdr antibody was performed for mouse proximal small intestine tissue (mouse small intestine) and cultured organoids on Day 3 (organoid). Scale bars, 100 μm .

$$C_{in}(t) = \frac{P_{app,active} + P_{app,passive}}{P_{app,passive}} \cdot C_{out} + e^{-P_{app,passive} \frac{S}{Vol} t} \cdot \left(C_{in}(0) - \frac{P_{app,active} + P_{app,passive}}{P_{app,passive}} \cdot C_{out} \right) \quad (8)$$

The inner Rh123 concentrations calculated from the fluorescent intensities of each experiment were plotted and then fitted to the function characterized in Eq. (8) using curve fitting on MATLAB software (The MathWorks, Inc.). By applying this process to the dataset obtained from each organoid, we could retrieve two kinetic parameters A (nmol/cm^3) and B (s^{-1}) as indicated below:

$$A = \frac{P_{app,active} + P_{app,passive}}{P_{app,passive}} \cdot C_{out} \quad (9)$$

$$B = P_{app,passive} \cdot \frac{S}{Vol} \quad (10)$$

Substituting $4\pi r^2$ and $4\pi r^3/3$ (r denotes the radius of organoid) into S and Vol , respectively, $P_{app,active}$ and $P_{app,passive}$ could be finally determined as below:

$$P_{app,passive} = \frac{B \cdot r}{3} \quad (11)$$

$$P_{app,active} = \frac{A - C_{out}}{C_{out}} \cdot P_{app,passive} = \frac{r}{3} \cdot B \cdot \frac{A - C_{out}}{C_{out}} \quad (12)$$

2.6. Statistical analysis

Data were presented as means \pm s.e. Statistical analysis was performed using the Student's t-test or Welch's t-test (Fig. 4C). Statistical significance for comparisons was assigned at $P < 0.01$ (Fig. 4C).

3. Results

First we assessed the expression of P-gp in intestinal epithelium obtained from murine small intestine and three-dimensionally

cultured. As previously described [17], they grew as epithelial organoids showing round cystic structures on Day 3, and then formed asymmetric structures having growing crypt-like protrusions on Day 5 (Fig. 1A). In the mouse, P-gp is encoded by two genes, *Abcb1a* and *Abcb1b*. We could detect the expression of *Abcb1a* in the intestinal tissue by our semi-quantitative RT-PCR (Fig. 1B), while *Abcb1b* mRNA was hardly detectable even with a high number of amplification cycles (data not shown). This supported the previous finding that *Abcb1a* is the major species of P-gp expressed in the small intestine [18]. In the cultured organoids, expression of *Abcb1a* stayed unchanged on Day 3 compared with that of isolated crypts on Day 1, whereas a slight decrease in its expression was noted on Day 5 (Fig. 1B). We also tested the expression of P-gp protein. Immunostaining with an antibody,

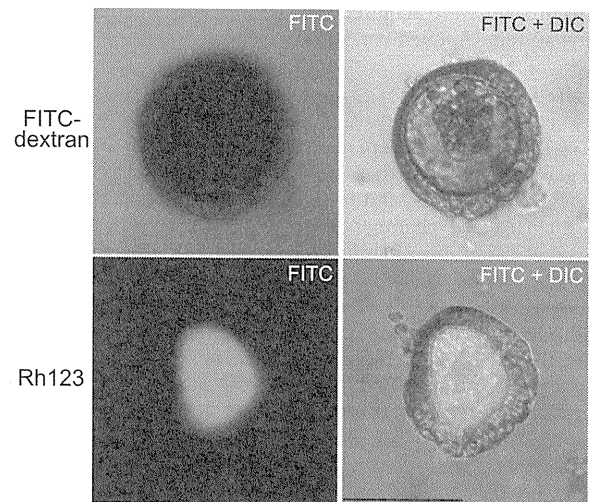


Fig. 2. Cultured organoids actively transport Rh123, while keeping their epithelial integrity. FITC-dextran (2mM, top) or Rh123 (1 μM , bottom) was added to the culture medium on Day 3, and images were acquired 5 h after the addition of the fluorescent probes. Fluorescent images (FITC) and their merged ones with DIC (FITC + DIC) are shown. Scale bar, 100 μm .

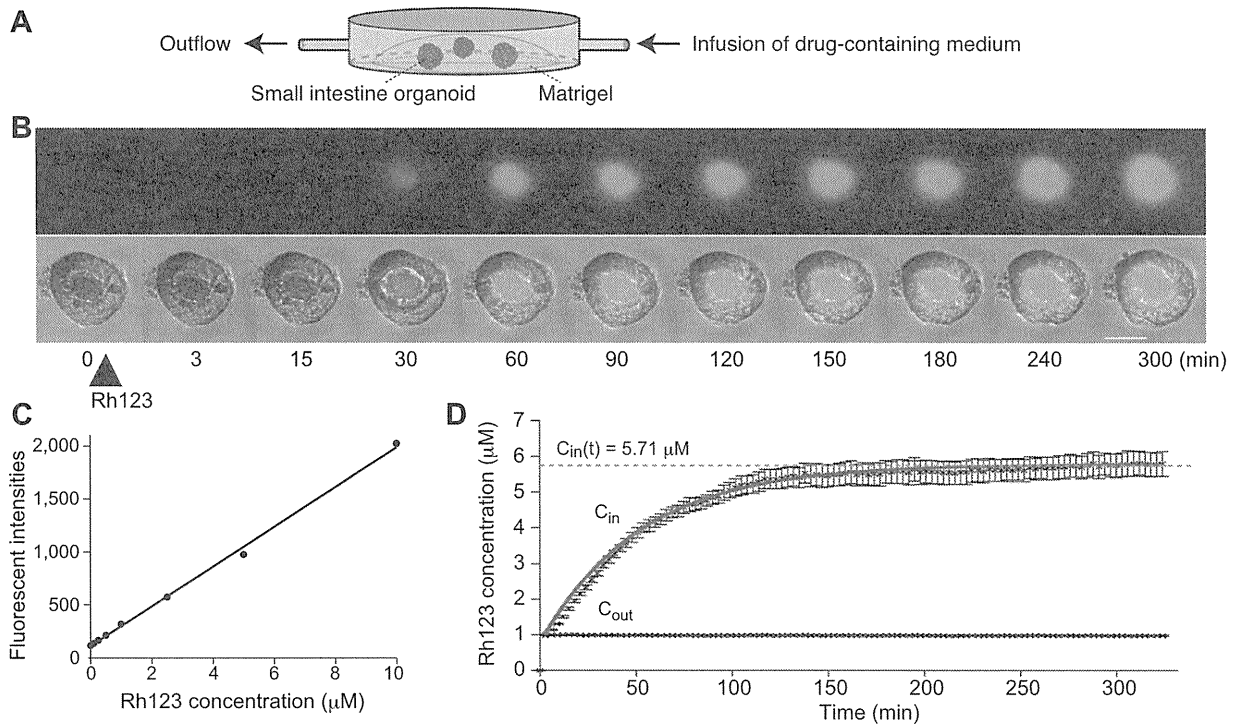


Fig. 3. Dynamics of Rh123 transport by cultured organoids and its mathematical modeling. (A) A schematic representation of the closed perfusable micro-observation chamber used for the time-lapse imaging. (B) Still images from time series of a Day 3 organoid actively transporting Rh123. Time 0 denotes the time frame immediately before the perfusion of Rh123. Fluorescent (FITC) images and their merged ones with DIC (FITC + DIC) are shown. Scale bar, 50 μm . The whole images can be viewed as Supplementary Video 1. (C) The linear correlation between the fluorescent intensity (expressed in arbitrary units) and Rh123 concentration under cell-free condition of the same experimental setting. (D) Rh123 concentrations inside and outside of organoids were calculated from data obtained by time-lapse experiments and plotted as mean \pm s.e. ($n = 10$). A curve obtained by fitting a mathematical model to data is shown in red. (For interpretation of the references to colour in this figure legend, the reader is referred to the web version of this article.)

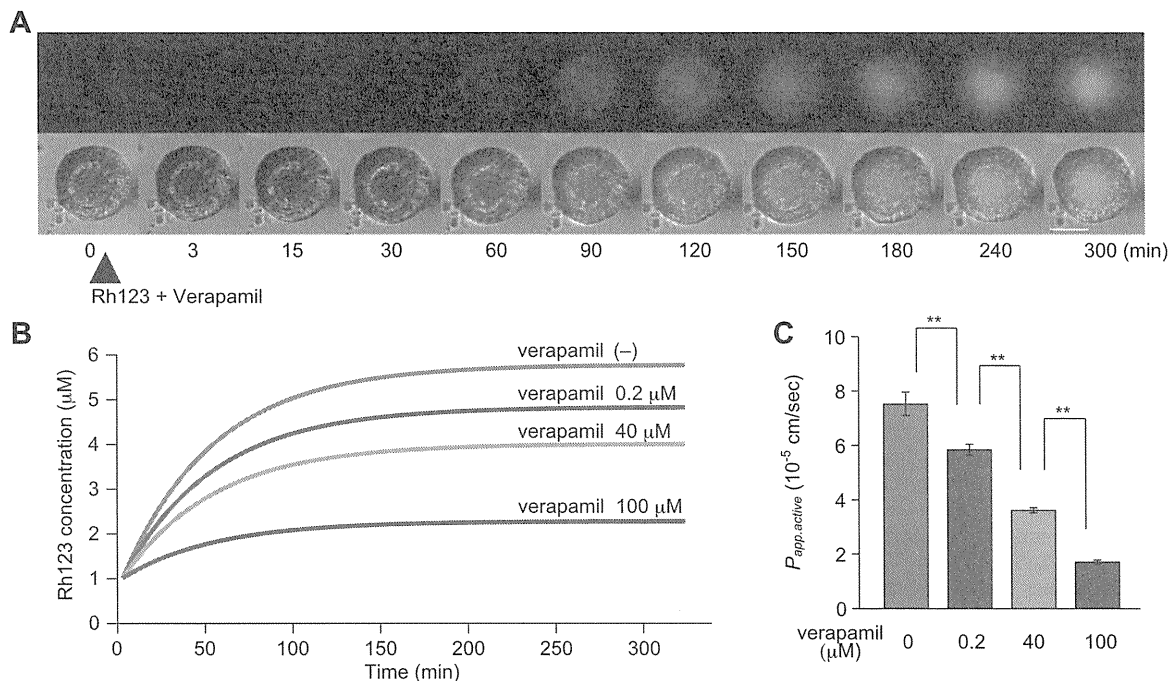


Fig. 4. Verapamil inhibits Rh123 transport across primary intestinal epithelium. (A) Time-lapse imaging experiments were performed as described in Fig. 3 in the presence of 40 μM verapamil. Fluorescent (FITC) and merged (FITC + DIC) images of a representative movie are shown. Scale bar, 50 μm . The video including these data, and other videos of the representative organoids recorded in the presence of 0.2 and 100 μM verapamil can be viewed as Supplementary Videos 2–4. (B) The curves obtained by fitting the mathematical model to data of verapamil inhibition experiments. (C) The $P_{app,active}$ values at various doses of verapamil were calculated and shown as mean \pm s.e. ($n = 10$ for each) ** $P < 0.01$.